

SPIRE Spectrometer Pipeline Description

SPIRE-BSS-DOC-002966

Trevor Fulton

**Version 1.4
26 September 2007**



SPIRE Spectrometer Pipeline Description

Trevor Fulton

Table of Contents

1. Introduction	1
1.1. Acronyms	1
1.2. Scope of Document	1
1.3. Documents	2
1.3.1. Applicable Documents	2
1.3.2. Reference Documents	2
1.4. Document History	2
2. SPIRE Spectrometer Pipeline Overview	3
2.1. Basic Pipeline Overview	3
2.2. Detailed Pipeline Overview	4
3. Spectrometer Pipeline	6
3.1. First Level Deglitching	6
3.2. Clipping Correction	6
3.3. Time Domain Phase Correction	7
3.4. Non-Linearity Correction	8
3.5. Interferogram Creation	8
3.6. SCAL and Telescope Correction	10
3.7. Baseline Correction	10
3.8. Second Level Deglitching	11
3.9. Channel Fringe Correction	11
3.10. Phase Correction	11
3.11. Apodization	13
3.12. Fourier Transform	13
3.13. Spectral Response Correction	15
3.14. Spectral Averaging	15
A. Appendix	16
A.1. First Level Deglitching Description	16
A.2. Radiation Incident on the SPIRE Spectrometer Detectors	17
A.3. Double-sided and Single-sided Interferograms	21
A.3.1. Double-sided Interferograms	21
A.3.2. Single-sided Interferograms	21

Chapter 1. Introduction

1.1. Acronyms

Table 1.1. Acronyms

Short Form	Full Name
ADC	Analog to Digital Converter
FFT	Fast Fourier Transform
FT	Fourier Transform
FTS	Fourier Transform Spectrometer
iFTS	Imaging Fourier Transform Spectrometer
ILS	Instrument Line Shape
LHS	Left Hand Side
LPF	Low Pass Filter
MPD	Mechanical Path Difference
NHKT	Nominal HouseKeeping Timeline Product
OPD	Optical Path Difference
QCP	Quality Control Pipeline
RHS	Right Hand Side
RMS	Root Mean Square
RSRF	Relative Spectral Response Function
SBS	Spectrometer Beam Splitter
SCAL	Spectrometer Calibrator
SDI	Spectrometer Detector Interferogram Product
SDS	Spectrometer Detector Spectrum Product
SDT	Spectrometer Detector Timeline Product
SLW	Spectrometer Long Wavelength Detector Array
SMEC	SPIRE Spectrometer Mechanism
SMECT	Spectrometer Mechanism Timeline Product
SPG	Standard Product Generation
SPIRE	Spectral and Photometric Imaging REceiver
SSW	Spectrometer Short Wavelength Detector Array
TBD	To Be Determined
TBW	To Be Written
WTMML	Wavelet Transform Modulus Maxima Lines
ZPD	Zero Path Difference

1.2. Scope of Document

This purpose of this document is to present an outline of the processing steps in the SPIRE spectrometer pipeline. The processing modules presented in this document follow those presented in Section 3 of [AD01], which describes the steps that are common to both the SPIRE spectrometer and photometer pipelines.

1.3. Documents

1.3.1. Applicable Documents

AD01	M Griffin, The SPIRE Analogue Signal Chain and Photometer Detector Data Processing Pipeline, SPIRE-UCF-REP-00****, DRAFT, 27 April 2007.
AD02	SPIRE Observers' Manual, HERSCHEL-HSC-DOC-0789, Version 1.0, 01 February 2007.
AD03	K. J. King, SPIRE Data Product Definition

1.3.2. Reference Documents

RD01	T. L. Lim, SPIRE Pipeline Description, SPIRE-RAL-DOC-002437
RD02	Jean-Paul Baluteau, PFM3b data: some SMEC or FTS performances, Presentation to SDAG 15, 10 July 2006

1.4. Document History

Table 1.2. Version and Date

Issue	Date
Draft 0.1	27 March 2007
Draft 0.2	02 May 2007
Version 1.0	09 May 2007
Version 1.1	27 June 2007
Version 1.2	10 July 2007
Version 1.3	31 August 2007

Chapter 2. SPIRE Spectrometer Pipeline Overview

2.1. Basic Pipeline Overview

The purpose of the SPIRE spectrometer data processing pipeline is to transform the spectrometer detector samples acquired during a single building block of a single SPIRE spectrometer observation into a set of spectra. In scanning mode, a building blocks consists of a set of scans of the spectrometer mechanism of the same resolution, with each scan defined as a single movement of the mechanism from one extreme position to the other.

The first steps of the SPIRE spectrometer and photometer pipeline are identical and are described in Section 3 of [AD01]. The SPIRE spectrometer pipeline modules that follow from that common processing pipeline collectively perform five basic operations, which are listed below:

1. **Modify Timelines**

The processing modules in this group perform time domain operations on the spectrometer detector samples.

2. **Create Interferograms**

The processing modules in this group merge the timelines of the spectrometer detectors and spectrometer mechanism into interferograms. The spectrometer detector samples are split into different sets, with each set defined by a single scan of the spectrometer mechanism.

3. **Modify Interferograms**

The processing modules in this group perform operations on the spectrometer detector interferograms. These operations differ from those in the "Modify Timelines" group in that they are designed to act on spatial domain data rather than time domain data.

4. **Transform Interferograms**

The processing modules in this group transform the interferograms into a set of spectra.

5. **Modify Spectra**

The processing modules in this group perform operations on the spectrometer detector spectra.

The manner in which the basic operations relate to one another is shown in Figure 2.1.

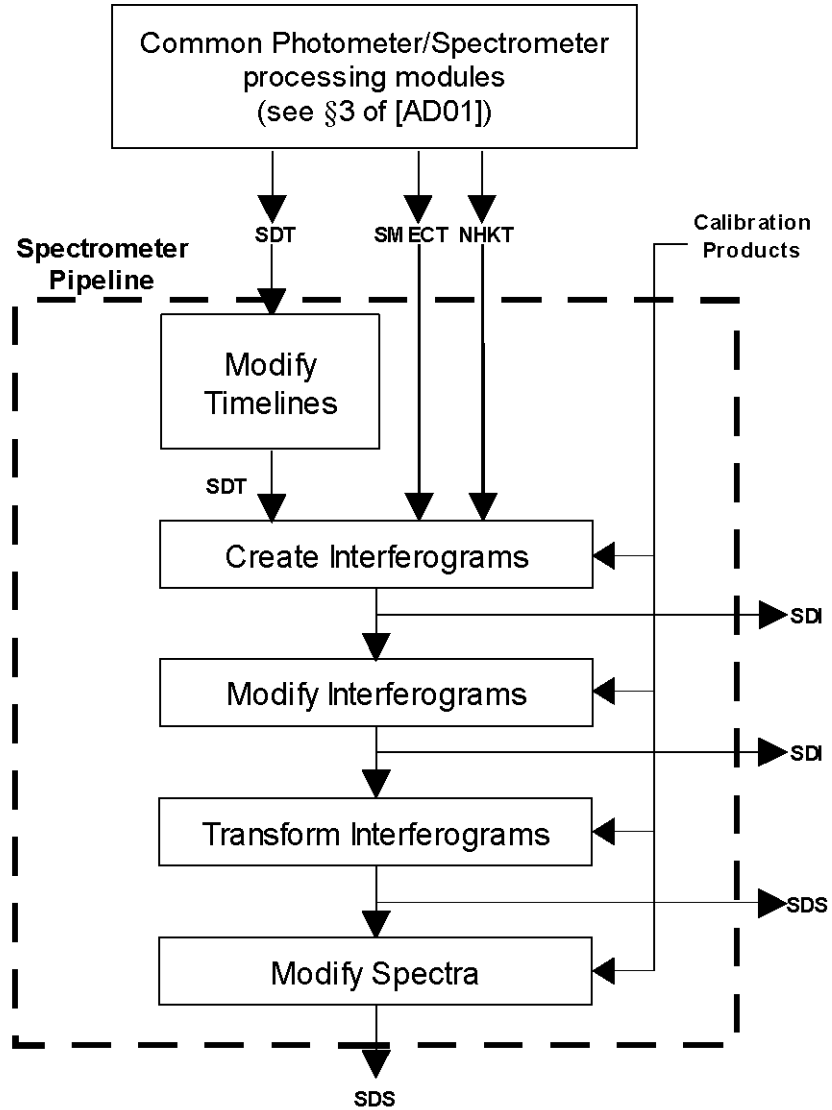


Figure 2.1. Basic Processing Operations of the SPIRE Spectrometer Pipeline

2.2. Detailed Pipeline Overview

The individual processing modules in the SPIRE spectrometer pipeline and their connection with one another are shown in Figure 2.2. Descriptions of the current implementation of these processing modules are presented in Chapter 3.

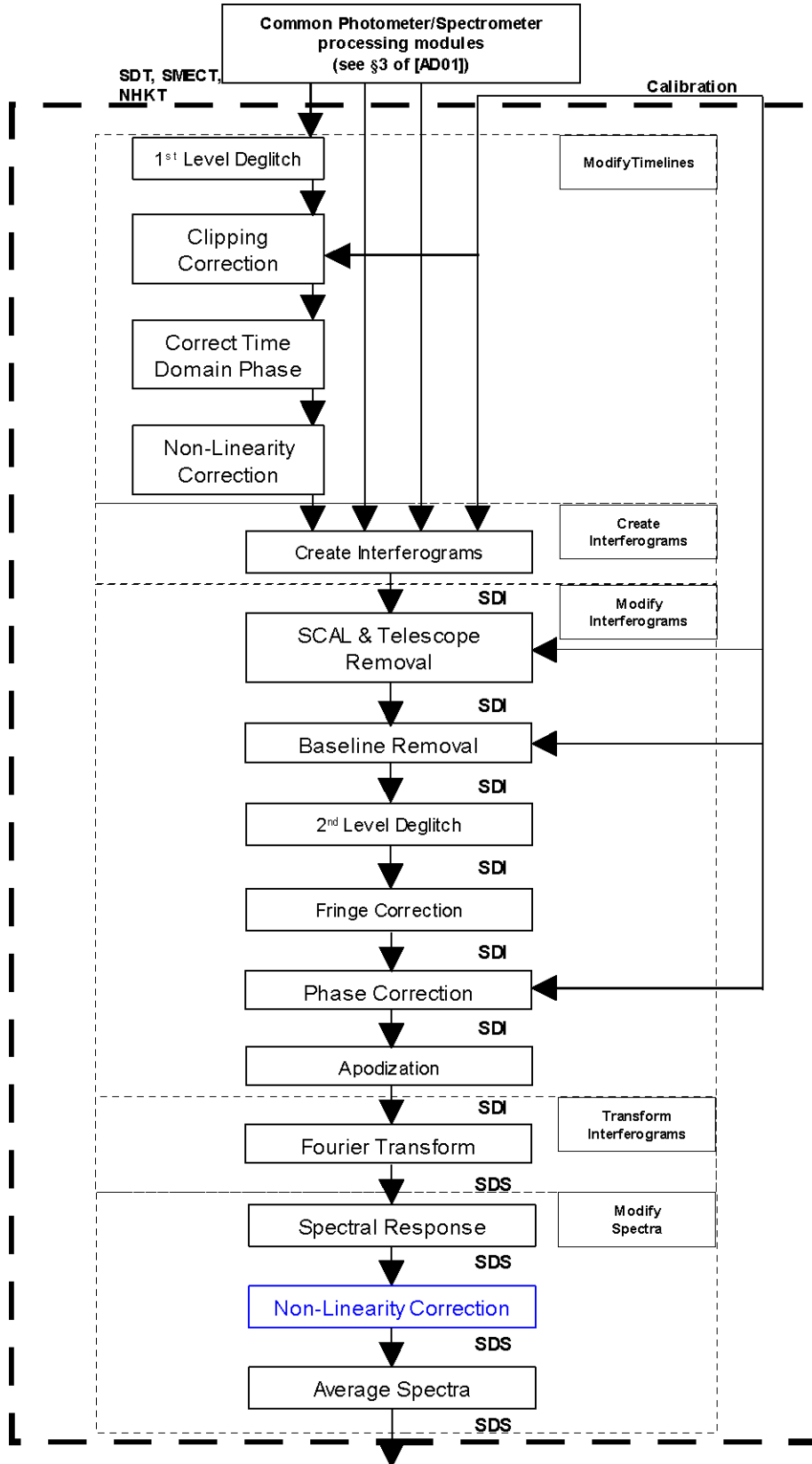


Figure 2.2. Detailed functionality of the SPIRE Spectrometer pipeline.

Chapter 3. Spectrometer Pipeline

3.1. First Level Deglitching

This module identifies and removes glitches from the spectrometer detector timelines or from the spectrometer detector interferograms. The method employed merges a local regularity analysis with a wavelet analysis.

This task is composed of two steps: the first step detects the glitch signatures over the measured signal; the second step locally reconstructs the signal by removing the glitch signatures. Each of these steps is discussed briefly below with a more detailed description as well as a discussion of the optimization of this algorithm provided in Section A.1.

1. **Glitch Identification.** Glitches are detected in the input SDT timeline by wavelet analysis noting that the glitch signature should be similar to signature of a dirac delta function.
2. **Glitch Removal.** Each glitch flagged by the preceding step is contains localized wavelet coefficients specific to the glitch. The glitches are removed by removing the glitch coefficients from the overall wavelet transform of the SDT.

3.2. Clipping Correction

The purpose of this processing step is to correct for clipping of the measured signals due to the limited range of the detector ADCs.

The presence of clipped signals in the SDT are problematic as they essentially represent missed samples in the timeline. If left uncorrected, this missed or erroneous samples can lead to further complications in particular when the timelines are converted into interferograms (Section 3.5).

Missed or erroneous samples can be corrected in a given SDT timeline as long as the number of consecutive missed samples SDT does not result in a violation of the Nyquist criteria. For sampled signals the Nyquist frequency defines the maximum independent frequency that is sampled. Using the nominal SPIRE spectrometer scanning parameters, the Nyquist frequency exceeds the maximum SLW frequency by a factor of 6 and exceeds the maximum SSW frequency by a factor of 4. As such, the sampled signals can be completely reconstructed even in the absence of five consecutive samples for SLW and three consecutive samples for the SSW detectors.

The process by which clipped timelines are corrected is described below.

1. **Check the number of consecutive clipped samples in SDT timeline.** If the number of consecutive clipped samples does exceeds five for the SLW detectors or three for the SSW detectors then discontinue the correction and set the appropriate flag for the Quality Control Pipeline (QCP).
2. **Subsample the SDT timeline.** The SDT is subsampled by an integer multiple so that the clipped signals are omitted.
3. **Interpolate the subsampled SDT timeline.** Interpolation of the subsampled SDT is performed by first computing its spectrum. If the Nyquist criteria is satisfied then the in-band spectrum of the subsampled timeline will be identical to that of the original timeline. The subsampled spectrum is then padded with zeroes to the original Nyquist frequency. Finally, the inverse Fourier transform is applied to the padded spectrum in order to recover the signal at the original sampling rate.



| Note

Currently, any SDT that contains clipped signals is flagged for the QCP for further inspection. SPIRE spectrometer observations flagged in this manner will be investigated by the Quality Control engineer to see if any valid astronomical products can be derived.

3.3. Time Domain Phase Correction

As mentioned in Section 3.7 of AD01, the SPIRE spectrometer detector chain contains a 6-pole Bessel low pass filter (LPF) with an addition LPF the transfer function of which is shown below.

Equation 3.1.

$$H_{LPF-S}(\omega_S) = \left[\frac{2.87}{1 + 7.85 \times 10^{-3}(j\omega_S) + 16.03 \times 100^{-6}(j\omega_S)^2} \right] \times \left[\frac{1}{1 + 3.23 \times 10^{-3}(j\omega_S) + 400 \times 100^{-6}(j\omega_S)^2} \right] \times \left[\frac{1}{1 + 6.26 \times 10^{-3}(j\omega_S) + 14.65 \times 100^{-6}(j\omega_S)^2} \right] \times \left[\frac{1}{1 + 1 \times 10^{-4}(j\omega_S)} \right]$$

In addition to the electronic LPF, the thermal behaviour of the SPIRE bolometers can be modeled as a simple LPF with a detector-specific time constant, τ .

Equation 3.2.

$$H_{LPF-Thermal}(\omega) = \left[\frac{\omega_{Thermal}}{(j\omega) + \omega_{Thermal}} \right]$$

These two effects may be combined into a single detector transfer function, given by the following:

Equation 3.3.

$$H_{TOTAL}(\omega_S) = \left[\frac{2.87}{1 + 7.85 \times 10^{-3}(j\omega_S) + 16.03 \times 100^{-6}(j\omega_S)^2} \right] \times \left[\frac{1}{1 + 3.23 \times 10^{-3}(j\omega_S) + 400 \times 100^{-6}(j\omega_S)^2} \right] \times \left[\frac{1}{1 + 6.26 \times 10^{-3}(j\omega_S) + 14.65 \times 100^{-6}(j\omega_S)^2} \right] \times \left[\frac{1}{1 + 1 \times 10^{-4}(j\omega_S)} \right] \times \left[\frac{\omega_{Thermal}}{(j\omega) + \omega_{Thermal}} \right]$$

As noted in Section 3.7 of AD01, the LPFs will affect the magnitude of the signal recorded by the SPIRE detectors. In addition, the LPFs will induce a phase shift to the recorded signal. The overall phase imparted by the combined effects of the LPF and the thermal response is then given by:

Equation 3.4.

$$\phi_{TOTAL}(\omega_S) = \tan^{-1} \left[\frac{\Im(H_{TOTAL}(\omega_S))}{\Re(H_{TOTAL}(\omega_S))} \right]$$

The phase shift from the combination of the read-out electronics and the thermal response of the detectors manifests itself, to first order, as a delay in time of the recorded signal. This effect is particularly problematic in scanning mode, where the delay induced by the electronic and thermal phase can lead to errors in the interpolation of the detector signals onto the SMEC positions (see Section 3.5).

The measured detector timelines can be corrected by first characterizing the phase shift (as above) then by deriving a time domain phase correction function (PCF)

Equation 3.5.

$$PCF_t(t) = FT^{-1} \left[e^{-\phi_{TOTAL}(\omega_s)} \right]$$

Convolution of the measured detector timelines with the derived time domain phase correction function results in a corrected timeline.

Equation 3.6.

$$I_{Corrected}(t) = I_{Measured}(t) \otimes PCF_t(t)$$

3.4. Non-Linearity Correction

A correction will be required to account for changes in the responsivity of the detectors as a function of the intensity of the incident radiation. The details of this processing step are still TBD, but the current algorithm involves applying a correction similar to that described in Section 3.3 with the phase correction replaced by an amplitude correction.

In addition, while the correction for detector non-linearities has been identified as necessary, it is still TBD as to where in the SPIRE spectrometer pipeline this correction will take place. Currently, this module is part of the group of steps that modify the spectrometer detector timelines. It may turn out that this module should more properly be applied to the spectra.

3.5. Interferogram Creation

A SPIRE spectrometer observation in scanning mode consists of a series of scans of the spectrometer mechanism while the instrument is pointed at a given target. The sampling of the SPIRE spectrometer detectors and the spectrometer mechanism is decoupled; the two subsystems are sampled at different rates and at different times. In order to derive the source spectrum from the measured data, the spectrometer detector samples must be linked with the position of the SMEC in the form of interferograms. Additionally, the SMEC positions onto which the spectrometer samples are to be interpolated should be regularly-spaced in terms of optical path difference (OPD). The purpose of this step is to ensure proper transformation of the interferogram with the Discrete Fourier Transform.

The process by which interferograms are created involves two steps, each of which is described below.

1. **Interpolation of the SMEC timeline.** This step converts the spectrometer mechanism timeline from one that is non-uniform in position to one that is uniform in position.
 - a. **Establish an OPD position vector.** This step creates a common vector of OPD positions that will be the basis for the interferograms for all of the spectrometer detector pixels and for all of the scans in the observation. This common position vector will contain samples that are uniformly-spaced in terms of OPD position. A common set of OPD positions is desired as it will allow for easier scan-to-scan and detector-to-detector comparisons of the interferograms of the particular SPIRE spectrometer observation.

In order to maintain the independence of the spectrometer detector signal samples, the step size of the common OPD vector is chosen in such a way as to maintain the independence of the spectrometer detector signal samples. For an SDT sampling rate s [Hz] and a SMEC scanning speed v_{SMEC} [cm/s MPD], the position step size, δMPD in units of cm; is given by:

Equation 3.7.

$$\delta MPD = v_{SMEC} / s$$

This step is then converted such that it is in terms of OPD by the following relation

Equation 3.8.

$$\delta\text{OPD} = \text{INT}[4\delta\text{MPD}]$$

where $\text{INT}[\]$ denotes that the step size is rounded to the nearest integer in units of μm OPD and the factor of four is the nominal conversion between MPD and OPD for a Mach-Zehnder FTS. Using the nominal SPIRE spectrometer settings, this results in an OPD step size of 25 μm .

- b. **Map the common OPD position vector to a SMEC position vector.** This step maps the common OPD positions established in the preceding step to SMEC mechanical path difference positions. This step takes into account the position of ZPD and the step-size conversion factor. As such this step is performed separately for each detector channel.

Equation 3.9.

$$\text{MPD}_{\text{Channel}} = \frac{\text{OPD}}{f_{\text{Channel}}} + \text{ZPD}_{\text{Channel}}$$

- c. **Parse the measured SMEC timeline into discrete scans.** This step splits the actual SMEC timeline ($z(t_{\text{SMEC}})$) into a series of discrete timelines, each of which represents one scan. The delineation of the measured SMEC timeline is accomplished by comparing consecutive samples and finding those samples where the motion of mirror mechanism changed direction.
- d. **Interpolate the measured SMEC timelines onto the mapped SMEC timelines.** The next step is to determine, on a channel-by-channel and scan-by-scan basis, the times when the spectrometer mechanism reached the mapped SMEC positions. Since, for each detector channel, there is a 1:1 relationship between the mapped SMEC positions and the regularly-spaced OPD positions, this step effectively determines the times when the SMEC reached the regularly-spaced OPD positions

Equation 3.10.

$$\text{MPD}_{\text{Measured}}(t) \rightarrow \text{MPD}_{\text{Channel}}(t')$$

2. **Merge the spectrometer detector and the mapped SMEC timelines.** This step combines the signal samples from the timeline of a given spectrometer detector channel with the mapped SMEC timeline.
 - a. **Interpolation of the spectrometer detector timelines.** The spectrometer detector signal samples are mapped onto the times corresponding to the SMEC positions by way of interpolation. Since there is a 1:1 relationship between the mapped SMEC positions and their sample times, this interpolation effectively maps the spectrometer detector signal sampled to the regularly-spaced SMEC positions.

Equation 3.11.

$$I(T) \rightarrow I(t') \rightarrow I(\text{MPD}_{\text{Channel}}) \rightarrow I_{\text{Channel}}(\text{OPD})$$

3.6. SCAL and Telescope Correction

The equation for the total intensity of the radiation incident upon the spectrometer detectors shows that, in addition to radiation from the astronomical source, the detectors record a modulated signal from the Telescope and from each of the components of the spectrometer calibrator (SCAL). A processing step is required to remove these components from the measured interferogram.

Equation 3.12.

$$I_{On-Source}(x) = (I_{Source}(x) + I_{Telescope}(x) + I_{SCAL}(x) + I_{SCAL2}(x) + I_{SCAL4}(x))$$

The preferred method for correction of the telescope and SCAL components is to subtract from the measured interferogram a calibration observation wherein the telescope is pointed at blank sky. This calibration observation will also have both SCAL2 and SCAL4 set to the same levels as was the case for the on-source observation.

Equation 3.13.

$$I_{Blank-Sky}(x) = (I_{Telescope}(x) + I_{SCAL}(x) + I_{SCAL2}(x) + I_{SCAL4}(x))$$

Equation 3.14.

$$I_{Corrected}(x) = I_{On-Source}(x) - I_{Blank-Sky}(x)$$

An alternate method for the removal of the Telescope and SCAL contributions is to model their contributions by a combination of the measured temperature of each element and the measured transmission through the spectrometer for each emitting element. This method has the advantage of not requiring a blank-sky calibration observation though the precision of such a method cannot be evaluated until flight conditions are observed.

Regardless of the method chosen, the result of the SCAL and Telescope correction will be an interferogram whose principal component is radiation from the astronomical source.

3.7. Baseline Correction

According to the equations presented in Section A.2, the overall intensity incident on the SPIRE spectrometer detectors can be separated into two components: a component that is constant as a function of OPD; a component that is modulated as a function of OPD. As the offset term does not contain any spectral information, it may be removed without affecting the source spectrum.

On a detector-by-detector and scan-by-scan basis, the baseline correction algorithm evaluates and removes the offset portion of the derived interferogram. The preferred manner to evaluate the offset is to compute the Fourier Transform of the derived interferogram and focus on those frequencies that are less than the lowest in-band frequencies.

Equation 3.15.

$$I_{Baseline}(x) = FT^{-1} \left[FT \left(I_{TOTAL}(x) \right) \Big|_0^{\sigma < \sigma_l} \right]$$

Once evaluated, the baseline portion is removed from the measured interferogram by subtraction.

Equation 3.16.

$$I_{Corrected}(x) = I_{TOTAL}(x) - I_{Baseline}(x)$$

3.8. Second Level Deglitching

Localized artifacts in the interferograms, glitches, pose a serious problem for Fourier Transform Spectrometer observations. As such, a glitch that affects as few as one interferogram sample can adversely affect each and every spectral component. Glitches in an interferogram must therefore be identified and removed prior to transformation in order to avoid unwanted spectral artifacts. Glitches are identified for each spectrometer detector by comparing, on a position-by-position basis, the samples from one scan to those from all other scans in the same observation. The samples that deviate more than a prescribed amount from the median are flagged as glitches.

The samples that are identified as glitches are then removed and replaced. For a glitch at a given position for a given spectrometer detector, the value of the replacement sample is determined by the average of the samples from the other interferograms at that position.



Note

The two steps of the interferogram deglitching module rely on a statistical analysis of the measured interferograms. As such, a minimum number of interferograms will be required so that these statistics will be meaningful.

3.9. Channel Fringe Correction

The effect of channel fringes on spectrometer data is similar to that of glitches (Section 3.8). If left uncorrected the channel fringes will contaminate the measured spectrum. The same methods that identify and correct for glitches cannot be applied to channel fringes. The reasons for this are two-fold: each interferogram is expected to contain channel fringes; the localized spectral signatures of the fringes are not that different from those of the uncontaminated signal.

Currently, three different algorithms are being evaluated as possible methods to correct for channel fringes. These are:

1. **Apodization.** Apodization (Section 3.11) has been suggested as an alternate method of fringe correction. While the application of an apodization function can be used to remove spectral artifacts, it comes at a cost of reduced spectral resolution. Since the observed fringe features appear at the extreme high-resolution OPD end for the SLW array and at the extreme medium-resolution end for the SSW array, however, the reduced resolution is not expected to be significant for those observing modes.
2. **Interferogram Truncation.** This method of channel fringe removal involves truncating the interferogram prior to the channel fringe region. The drawback to this method is similar to that for apodization; reduced spectral resolution.
3. **Iterative Subtraction.** This method of channel fringe correction is performed by removing successive copies of the interferogram in the region near ZPD from the wing portion of the interferogram.

3.10. Phase Correction

The even symmetry of a Fourier Transform spectrometer theoretically implies that interferograms recorded by the spectrometer will also exhibit even symmetry. The spectrum of an evenly symmetric interferogram contains only real components, as per:

Equation 3.17.

$$FT[I_{Symmetric}(x)] = \int_{-\infty}^{\infty} I(x) e^{-i2\pi\sigma x} dx = B(\sigma) = B_{\Re}(\sigma)$$

The presence of dispersive elements and the possibility that the position of zero path difference not being sampled can result in a measured interferogram whose *signal* samples are not symmetric about ZPD. Left uncorrected, the spectrum calculated from this sort of asymmetric interferogram will contain both real and imaginary components.

Equation 3.18.

$$\begin{aligned} FT[I_{Asymmetric}(x)] &= \int_{-\infty}^{\infty} I(x) e^{-i2\pi\sigma x} dx \\ &= \int_{-\infty}^{\infty} I_{Even}(x) \cos(2\pi\sigma x) dx + i \int_{-\infty}^{\infty} I_{Odd}(x) \sin(2\pi\sigma x) dx \\ &= B_{\Re}(\sigma) + i B_{\Im}(\sigma) \\ &= B(\sigma) e^{i\phi(\sigma)} \end{aligned}$$

The phase correction process renders the measured interferogram *signal* symmetric about ZPD by moving the components of the spectrum that are located in the imaginary domain to the real domain.

If the interferograms are double-sided (see Section A.3.1) then the resultant spectra will contain phase information for each spectral element. As such, phase correction of these interferograms can take place solely in the spectral domain. The spectrum, $B(\sigma)$, can be corrected by way of multiplication with a phase correction function (PCF) as:

Equation 3.19.

$$B_{PC}(\sigma) = B(\sigma) e^{i\phi(\sigma)} \times PCF = B(\sigma) e^{i\phi(\sigma)} \times e^{-i\phi(\sigma)}$$

It should be noted that the PCF referred to here is not simply the negative of the measured phase. Rather, a fit is made to the measured in-band phase and it is complex exponential of the negative of this fit that is used as the PCF. The basis for using the fitted phase rather than the calculated phase is that, by doing so, the noise associated with the imaginary portion of the spectrum remains in the imaginary domain. For random sources of measurement noise and if the phase is stable, this can lead to an increase in the signal-to-noise ratio by a factor of $\sqrt{2}$.

For single-sided interferograms (Section A.3.2), phase correction is performed by first computing the uncorrected spectrum (magnitude and phase) from the double-sided subsets of the single-sided interferograms. The phase correction function (PCF) is derived from an intensity-weighted in-band fit to the measured phase. Since this PCF is derived from the low-resolution portion of the interferogram, it cannot be directly applied to the uncorrected single-sided spectrum. Single-sided phase correction, by contrast, proceeds in the interferogram (spatial) domain rather than the spectral domain. The PCF is not multiplied with the uncorrected spectrum, instead the inverse FT of the PCF is convolved with the uncorrected single-sided interferogram.

Equation 3.20.

$$I_{PC}(x) = I(x) \otimes PCF = I(x) \otimes FT^{-1}[e^{-i\phi(\sigma)}]$$

It should be noted that the operation expressed in the equation above is mathematically equivalent to that for double-sided interferograms since, from Fourier theory, multiplication in one domain is equivalent to convolution in the other domain. The sample *signals* in the interferogram that results from this convolution are rendered symmetric about ZPD. This symmetry means that only that portion of the single-sided interferogram where the optical path difference is greater than or equal to ZPD is required to compute the resultant spectrum.

3.11. Apodization

The natural instrument line shape (ILS) for a Fourier Transform spectrometer is a cardinal sine or Sinc function. For interferograms that contain features that are at or near the resolution of the spectrometer, the Sinc line shape can introduce secondary maxima in the calculated spectra. The apodization functions available within this module may be used by astronomers that wish to minimize these secondary maxima.

Apodization is performed by multiplying the spectrometer detector interferogram by a tapering or apodizing function prior to transformation. A consequence of apodization is that it leads to a reduction in the resolution of the resultant spectrum. To minimize the effect on spectral resolution, the apodization module in the SPIRE spectrometer data processing pipeline provides a number of functions that optimize the trade-off between reduction in the secondary maxima and reduced resolution.

3.12. Fourier Transform

The purpose of this module is to transform a set of interferograms from a SPIRE spectrometer observation into a set of spectra. In its current form, this processing module is capable of transforming both double-sided and single-sided interferograms (see Appendix A for the definition of double-sided and single-sided interferograms).

Double-sided Transform. For the double-sided transform, each spectrometer detector interferogram is examined and the double-sided portion of the interferogram is used to compute the resultant spectrum. The resultant spectra will contain both real and imaginary components.

Equation 3.21.

$$B(\sigma) = FT \left[I(x) \Big|_{-L}^L \right] = \int_{-L}^L I(x) e^{-i2\pi\sigma x} dx$$

In this case, the discrete fourier transform that is used to compute the spectral components takes the form shown in Equation 3.22.

Equation 3.22.

$$B_{DS}(k) = \sum_{n=0}^{N-1} I(n) e^{-i \frac{2\pi kn}{N}}$$

Single-sided Transform. In the case of the single-sided transform, only those interferogram samples to one side of the position of zero path difference are considered. The spectra that result from the single-sided transform therefore contain only real components.

Equation 3.23.

$$B(\sigma) = FT \left[I(x) \Big|_0^L \right] = \int_0^L I(x) e^{-i2\pi\sigma x} dx$$

The discrete fourier transform that is used to compute the spectral components for single-sided interferograms takes the form shown in Equation 3.24.

Equation 3.24.

$$B_{SS}(k) = \sum_{n=0}^{N-1} I(n) \cos \frac{2\pi kn}{N}$$

Wavenumber Grid. For both the single-sided and double-sided transforms the wavenumber grid onto which the spectrum is registered is calculated based on the interferogram sampling rate (ΔOPD) and on the displacement of the SMEC from the position of ZPD, L .

The Nyquist frequency ($\sigma_{Nyquist}$), the maximum independent frequency in the output spectrum, is given by:

Equation 3.25.

$$\sigma_{Nyquist} = \frac{1}{2\Delta x}$$

The spacing between independent spectral samples ($\Delta\sigma$) is given by:

Equation 3.26.

$$\Delta\sigma = \frac{1}{2L}$$

The spacing between spectral samples can be modified by padding the interferogram with zeroes. This procedure does not add any information to the spectrum but allows for an easier comparison between observations. In this case, the zero-padded interferogram (I_{ZP}) is given by:

Equation 3.27.

$$I_{ZP}(x) = I(x) \Big|_0^L, 0 \Big|^{L < x \leq L_{ZP}}$$

The corresponding spectral sampling interval is given by:

Equation 3.28.

$$\Delta\sigma_{ZP} = \frac{1}{2L_{ZP}}$$

and the resultant spectrum of the zero-padded interferogram is given by:

Equation 3.29.

$$B_{ZP}(k) = FT [I_{ZP}(n)] = \sum_0^{N_{ZP}-1} I(n) \cos \frac{2\pi kn}{N_{ZP}}$$

The scan lengths and resultant spectral sampling intervals for the three distinct spectral resolutions

from Section 6.6 of [AD02] are given in Table 3.1.

Table 3.1. Interferogram Padding

Spectral Resolution [AD02]	Sampling Interval (OPD) [μm]	Nyquist Wavenumber [cm^{-1}]	Scan Length (OPD) [cm]	Spectral Sampling Interval [cm^{-1}]
Low	25	200	1.25	0.4
Medium	25	200	5.0	0.01
High	25	200	12.5	0.04

3.13. Spectral Response Correction

This module will remove from each measured spectrum the effective transmission of the SPIRE instrument. Included in this step are corrections for the efficiencies of the aperture and the feedhorns, as well as the transmission of the waveguide, filters, beamsplitters, and mirrors.

Equation 3.30.

$$B_{\text{Measured}}(\sigma) = B_{\text{Source}}(\sigma) \times \text{SpectralResponse}(\sigma)$$

where:

Equation 3.31.

$$\text{SpectralResponse}(\sigma) = \eta_A(\sigma) \eta_{\text{feedhorn}}(\sigma) T_{\text{waveguide}}(\sigma) T_{\text{filters}}(\sigma) T_{\text{mirrors}}(\sigma) T_{\text{Beamsplitters}}(\sigma)$$

3.14. Spectral Averaging

This step in the SPIRE data processing pipeline averages the spectra from all scans for each detector pixel for a given observation. In the case of observations that feature a combination of high- and low-resolution scans, the low-resolution output average spectrum product will contain the spectra derived from the low-resolution portion of the high-resolution scans.

Appendix A. Appendix

A.1. First Level Deglitching Description

1. **Glitch Identification.** Glitch signatures are detected by performing a local regularity analysis (Holderian analysis) over the wavelet transform modulus maxima lines (WTMML) of the signal.

Let H be the Holder exponent, s the scale of decomposition, $X_i(s)$ the time (or OPD) domain coordinate of the maxima line for the scale s , then when the scale s goes to zero the corresponding wavelet coefficient, $W(X_i(s), s)$, is given by:

Equation A.1.

$$W(X_i(s), s) \leq C s^H$$

where C is a real constant.

The scale of decomposition, s , may be expressed over a logarithmic scale as:

Equation A.2.

$$s = 2^o 2^{v/nV}$$

where positive integers o , nV , and v (with $v < nV$) are respectively called octave, number of voices, and voice of the decomposition¹, respectively.

On each maxima line, the regularity degree of the signal is estimated by computing the slope of the linear regression over the set of points $(\log_2(|W|), \log_2(s))$ over the range of scales $[\text{scaleMin}, \text{scaleMax}]$. If the relation is linear, i.e. if the square of its correlation coefficient C is greater than the threshold coefficient *thresholdCorr* then the Holder exponent H can be estimated by the measure of the slope of the relation. Glitches are detected as they are similar to dirac-like signatures and show a Holder exponent (i.e. regularity degree) close to -1 , ie in a range $[\text{thresholdHolder}, \text{hMin}]$ centered over -1 .

Noise can generate false detections (it can be shown that the Holder exponent of a gaussian noise has a value (in mean) of 0.5). In order to minimize the likelihood of these false positives, constraints are applied to the wavelet coefficients. By considering a gaussian noise of standard deviation σ , it can be shown that at the lowest scale of decomposition, the following threshold :

Equation A.3.

$$|W| \leq \sigma \sqrt{2 \ln N}$$

where N is the size of the signal.

The noise standard deviation σ on the signal can be estimated using the Donoho estimator; at the lowest scale, $\sigma = 0.6745 \times \text{med } |W|$

For each maxima line, if the value of the wavelet coefficient for the first scale value is greater than the previous threshold an estimate is made of the regularity degree.

Glitch Removal. Each glitch flagged by the preceding step is characterized by a Holder exponent H and by a maxima line X giving for each scale s the location of the maximum of the modulus of the wavelet coefficient $X(s)$. For a glitch signature (the Holder exponent $H \sim -1$), it can be shown that the wavelet coefficients W_g are given by:

¹ C.Ordenovic, C. Surace, B. Torresani, A. Llebaria, JP. Baluteau, "Use of a local regularity analysis by a wavelet analysis for glitches detection", Proc. SPIE Vol. 5909 (2005), 556-567.

Equation A.4.

$$W_g = \psi((b-X(s)) / s)$$

ψ being the wavelet function.

The glitch coefficients, W_g , are then subtracted from the wavelet coefficients, W , and the signal is locally reconstructed by performing a wavelet transform over the corrected wavelet coefficients.

The parameters that follow are optional and have been optimized for the SPIRE spectrometer detectors. SPIRE PFM1 data that, by visual inspection, contained 29 glitches was used as a basis for this optimization.

- **scaleMin, scaleMax**: The scale range used for the linear regression. Optimal values are scaleMin = 2 and scaleMax = 8.
- **thresholdHolder and H_{\min}** : The Holder exponent range used to select a glitch. Optimal values are thresholdHolder = -0.6, $H_{\min} = -1.3$.
- **thresholdCorr**: The square threshold correlation that defines linear behaviour. The optimal value is thresholdCorr = 0.985.
- **voices**: The number of voices used for the scale decomposition. The optimal value is voices = 5.

A.2. Radiation Incident on the SPIRE Spectrometer Detectors

The radiation path through the SPIRE spectrometer is illustrated for one case in Figure A.1.

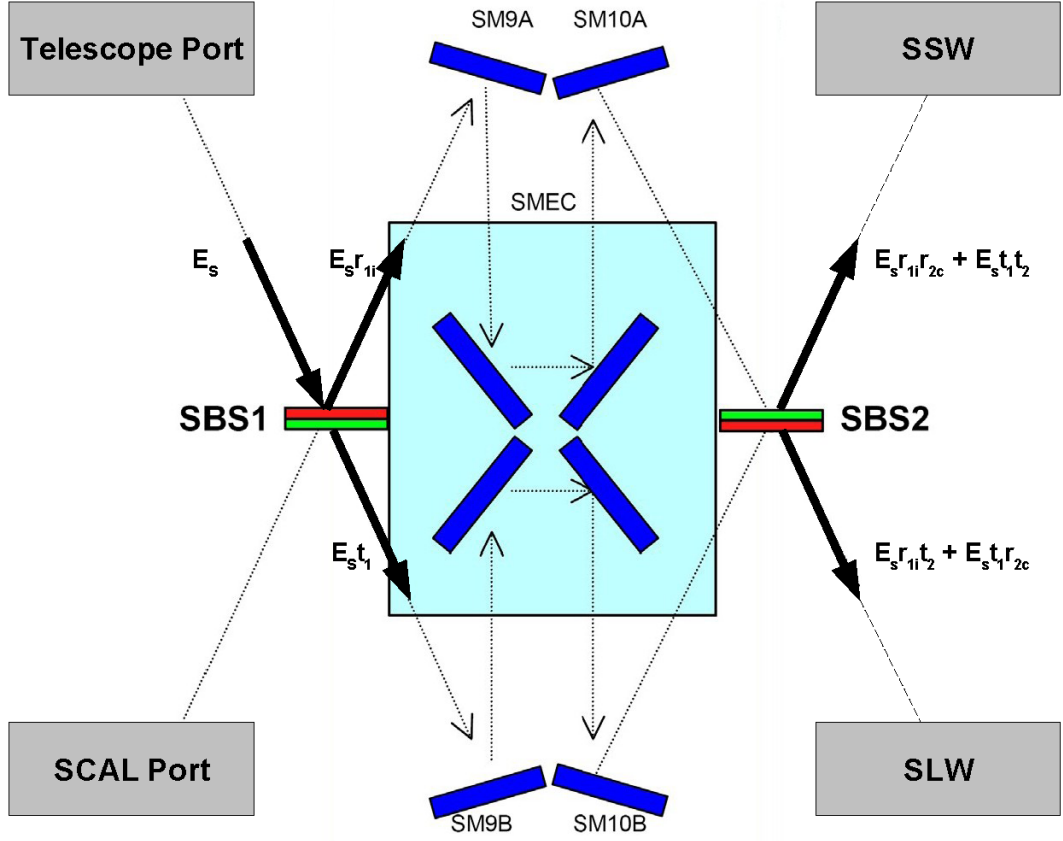


Figure A.1. Radiation from an astronomical source through the SPIRE spectrometer

As shown in Figure A.1, the first beamsplitter (SBS1) divides the incoming electric field (E_s) into two components (E_{s1c} and E_{s1t}). These two components pass through the interferometer and then are split further at the second beamsplitter (SBS2). The upper beam from Figure A.1 then passes to the SSW detectors while the lower beam passes to the SLW detectors. The electric fields incident on the SSW and SLW detectors are given by the following equations:

Equation A.5.

$$E_{S-SSW}(x, \sigma) = E_{S_0}(\sigma) \left[r_1 r_2 e^{-i2\pi(\sigma x_1 - vt)} + t_1 t_2 e^{-i2\pi(\sigma x_2 - vt)} \right]$$

Equation A.6.

$$E_{S-SLW}(x, \sigma) = E_{S_0}(\sigma) \left[r_1 t_2 e^{-i2\pi(\sigma x_1 - vt)} + t_1 r_2 e^{-i2\pi(\sigma x_2 - vt)} \right]$$

At the detectors, the intensity recorded is the time-average of the square of the incident electric field. Using the SSW detectors for illustration, the measured intensity for radiation from an astronomical source at the detectors is given by the following:

Equation A.7.

$$I_S(x, \sigma) = \frac{c \epsilon_0}{2} E_S^*(x, \sigma) E_S(x, \sigma)$$

where:

Equation A.8.

$$E_S^*(x, \sigma) E_S(x, \sigma) = E_{S_0}^*(\sigma) \left[r_1 r_2 e^{i2\pi(\sigma x_1)} + t_1 t_2 e^{i2\pi(\sigma x_2)} \right] \times E_{S_0}(\sigma) \left[r_1 r_2 e^{-i2\pi(\sigma x_1)} + t_1 t_2 e^{-i2\pi(\sigma x_2)} \right]$$

Equation A.9.

$$E_S^*(x, \sigma) E_S(x, \sigma) = E_{S_0}^2(\sigma) \left[(r_1 r_2)^2 + (t_1 t_2)^2 + 2 r_1 r_2 t_1 t_2 \cos 2\pi \sigma (x_1 - x_2) \right]$$

Combining the above results in the following equations for the measured intensity at the SSW and SLW detectors for radiation from an astronomical source:

Equation A.10.

$$\begin{aligned} I_{SSW}(x) &= \int_0^\infty I_{SSW}(x, \sigma) d\sigma \\ &= \int_0^\infty E_0^2(\sigma) \left[(r_1 r_2)^2 + (t_1 t_2)^2 + 2 r_1 r_2 t_1 t_2 \cos(2\pi \sigma x) \right] d\sigma \\ &= I_{SSW}(0) \left[(r_1 r_2)^2 + (t_1 t_2)^2 \right] + 2 \int_0^\infty [r_1 r_2 t_1 t_2] B(\sigma) \cos(2\pi \sigma x) d\sigma \\ &= I_{SSW-Offset} + I_{SSW-Modulated}(x) \end{aligned}$$

Equation A.11.

$$\begin{aligned} I_{SLW}(x) &= \int_0^\infty I_{SLW}(x, \sigma) d\sigma \\ &= \int_0^\infty E_0^2(\sigma) \left[(r_1 t_2)^2 + (t_1 r_2)^2 - 2 r_1 r_2 t_1 t_2 \cos(2\pi \sigma x) \right] d\sigma \\ &= \left[(r_1 t_2)^2 + (t_1 r_2)^2 \right] I_{SSW}(0) - 2 \int_0^\infty [r_1 r_2 t_1 t_2] B(\sigma) \cos(2\pi \sigma x) d\sigma \\ &= I_{SLW-Offset} + I_{SLW-Modulated}(x) \end{aligned}$$

In addition to the astronomical source, radiation from the Herschel telescope and the three components of SCAL (SCAL2, SCAL4, and SCAL) is incident on the SPIRE spectrometer detectors. For the telescope radiation, its path through the SPIRE spectrometer is the same as that for the astronomical source. The path for the SCAL emitters is slightly different (see Figure A.1). The equations for the radiation incident on the SSW and SLW detectors are given by the following:

Equation A.12.

$$\begin{aligned}
 I_{SSW}(x) &= \int_0^{\infty} I_{SSW}(x, \sigma) d\sigma \\
 &= \int_0^{\infty} E_0^2(\sigma) \left[(r_{1_c} t_2)^2 + (t_1 r_{2_c})^2 - 2 r_{1_c} r_{2_c} t_1 t_2 \cos(2\pi \sigma x) \right] d\sigma \\
 &= \left[(r_{1_c} t_2)^2 + (t_1 r_{2_c})^2 \right] I_{SSW}(0) - 2 \int_0^{\infty} [r_{1_c} r_{2_c} t_1 t_2] B(\sigma) \cos(2\pi \sigma x) d\sigma \\
 &= I_{SSW-Offset} + I_{SSW-Modulated}(x)
 \end{aligned}$$

Equation A.13.

$$\begin{aligned}
 I_{SLW}(x) &= \int_0^{\infty} I_{SLW}(x, \sigma) d\sigma \\
 &= \int_0^{\infty} E_0^2(\sigma) \left[(r_{1_c} r_{2_c})^2 + (t_1 t_2)^2 + 2 r_{1_c} r_{2_c} t_1 t_2 \cos(2\pi \sigma x) \right] d\sigma \\
 &= \left[(r_{1_c} r_{2_c})^2 + (t_1 t_2)^2 \right] I_{SSW}(0) + 2 \int_0^{\infty} [r_{1_c} r_{2_c} t_1 t_2] B(\sigma) \cos(2\pi \sigma x) d\sigma \\
 &= I_{SLW-Offset} + I_{SLW-Modulated}(x)
 \end{aligned}$$

Taken together, the overall intensity of the radiation measured by the SPIRE spectrometer detectors is given by the following:

Equation A.14.

$$I_{TOTAL}(x) = I_{Source}(x) + I_{Telescope}(x) + I_{SCAL}(x) + I_{SCAL2}(x) + I_{SCAL4}(x)$$

1. **SSW Detectors.**

Equation A.15.

$$\begin{aligned}
 I_{SSW}(x) &= (I_{Source}(0) + I_{Telescope}(0)) \left[(r_{1_c} r_{2_c})^2 + (t_1 t_2)^2 \right] + (I_{SCAL}(0) + I_{SCAL2}(0) + I_{SCAL4}(0)) \left[(r_{1_c} t_2)^2 + (t_1 r_{2_c})^2 \right] \\
 &\quad + 2 \int_0^{\infty} [r_{1_c} r_{2_c} t_1 t_2] B_{Source}(\sigma) \cos(2\pi \sigma x) d\sigma + 2 \int_0^{\infty} [r_{1_c} r_{2_c} t_1 t_2] B_{Telescope}(\sigma) \cos(2\pi \sigma x) d\sigma \\
 &\quad - 2 \int_0^{\infty} [r_{1_c} r_{2_c} t_1 t_2] B_{SCAL}(\sigma) \cos(2\pi \sigma x) d\sigma - 2 \int_0^{\infty} [r_{1_c} r_{2_c} t_1 t_2] B_{SCAL2}(\sigma) \cos(2\pi \sigma x) d\sigma \\
 &\quad - 2 \int_0^{\infty} [r_{1_c} r_{2_c} t_1 t_2] B_{SCAL4}(\sigma) \cos(2\pi \sigma x) d\sigma
 \end{aligned}$$

2. **SLW Detectors.**

Equation A.16.

$$\begin{aligned}
 I_{SLW}(x) = & (I_{Source}(0) + I_{Telescope}(0)) \left[(r_1 t_2)^2 + (t_1 r_2)^2 \right] + (I_{SCAL}(0) + I_{SCAL2}(0) + I_{SCAL4}(0)) \left[(r_1 r_2)^2 + (t_1 t_2)^2 \right] \\
 & - 2 \int_0^{\infty} [r_1 r_2 t_1 t_2] B_{Source}(\sigma) \cos(2\pi \sigma x) d\sigma - 2 \int_0^{\infty} [r_1 r_2 t_1 t_2] B_{Telescope}(\sigma) \cos(2\pi \sigma x) d\sigma \\
 & + 2 \int_0^{\infty} [r_1 r_2 t_1 t_2] B_{SCAL}(\sigma) \cos(2\pi \sigma x) d\sigma + 2 \int_0^{\infty} [r_1 r_2 t_1 t_2] B_{SCAL2}(\sigma) \cos(2\pi \sigma x) d\sigma \\
 & + 2 \int_0^{\infty} [r_1 r_2 t_1 t_2] B_{SCAL4}(\sigma) \cos(2\pi \sigma x) d\sigma
 \end{aligned}$$

A.3. Double-sided and Single-sided Interferograms

The terms double-sided and single-sided as used in this document describe the two types of interferograms that can be measured with a Fourier Transform Spectrometer.

A.3.1. Double-sided Interferograms

Double-sided interferograms are defined as those interferograms or that portion of measured interferogram where the sample *positions* are symmetric about the position of zero path difference (ZPD). That is, a double-sided interferogram is one that contains an equal number of samples before and after the ZPD sample². An envelope of a double-sided interferogram is shown in Figure A.2.

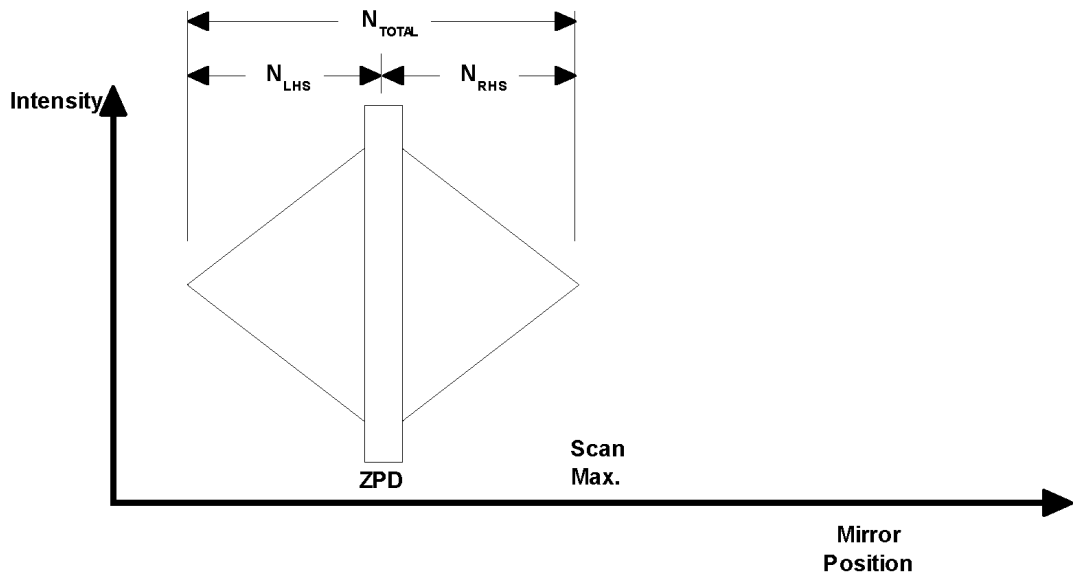


Figure A.2. Envelope of a double-sided interferogram

A.3.2. Single-sided Interferograms

Single-sided interferograms are defined as those interferograms that contain more samples on one side of ZPD than the other. An envelope of a single-sided interferogram is shown in Figure A.3.

² Some implementations of the Fourier Transform may require an even number of points (N_{TOTAL} even). In this case, the RHS of the double-sided interferogram will contain an extra point to render the total number of points even.

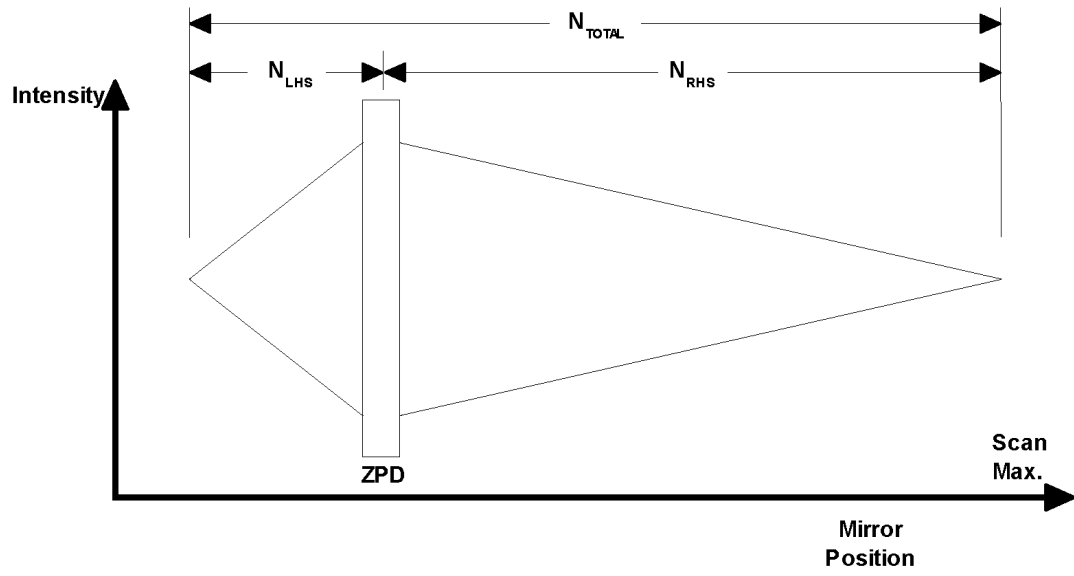


Figure A.3. Envelope of a single-sided interferogram